Published in final edited form as:
Magn Reson Imaging. 2013 September ; 31(7): 1097–1104. doi:10.1016/j.mri.2013.03.020.

White matter maturation in the brains of Long Evans shaker myelin mutant rats by ex-vivo QSI and DTI

Debbie Anaby[a], **Ian D. Duncan**[b], **Chelsey M. Smith**[b], and **Yoram Cohen**[a,c,*]

[a]School of Chemistry, Sackler Faculty of Exact Sciences, Tel Aviv University, Tel Aviv, Israel

[b]Department of Medical Sciences, School of Veterinary Medicine, University of Wisconsin-Madison, Madison, WI, USA

[c]Sagol School of Neurosciences, Tel Aviv University, Tel Aviv, Israel

Abstract

The brains of Long Evans shaker (*les*) rats, a model of dysmyelination, and their age- matched controls were studied by ex-vivo q-space diffusion imaging (QSI) and diffusion tensor imaging (DTI). The QSI and DTI indices were computed from the same acquisition. The *les* and the control brains were studied at different stages of maturation and disease progression. The mean displacement, the probability for zero displacement and kurtosis were computed from QSI data while the fractional anisotropy (FA) and the eigenvalues were computed from DTI. It was found that all QSI indices detect the *les* pathology, at all stages of maturation, while only some of the DTI indices could detect the *les* pathology. The QSI mean displacement was larger in the *les* group as compared with their age-matched controls while the probability for zero displacement and the kurtosis were both lower all indicating higher degree of restriction in the control brains. Since all the DTI eigenvalues were higher in the *les* brains as compared to controls, the less efficient DTI measure for discerning the *les* pathology was found to be the FA. Clearly, the most sensitive DTI parameter to the *les* pathology is λ_3, i.e. the minimal diffusivity. Since the QSI and DTI data were obtained from the same acquisition, despite the somewhat higher SNR of the QSI data compared to the DTI data, it seems that the higher diagnostic capacity of the QSI data in this experimental model of dysmyelination, originates mainly from the higher diffusing weighting of the QSI data.

Keywords

Myelin; Diffusion; MRI; Long Evans shaker; DTI; Rat; Brain; Q-space diffusion MRI; QSI; Restricted diffusion; Diffusion anisotropy

*Corresponding author. School of Chemistry, The Raymond and Beverly Sackler Faculty of Exact Sciences, Tel Aviv University, Ramat Aviv, Tel Aviv 69978, Israel. Tel.: +972 3 6407232; fax: +972 3 6407469. ycohen@post.tau.ac.il. .

1. Introduction

Diffusion weighted imaging and diffusion tensor magnetic resonance imaging (DWI and DTI, respectively) which measure the Brownian motion of water molecules, have become one of the most important MR imaging modalities of the central nervous system (CNS). These methods can be used to study brain pathologies and microstructures [1–3]. In grey matter (GM), the bodies of neural cells and dendrites are not arranged in a directional manner and the macroscopic water diffusion is largely isotropic. In white matter (WM), however, the bundles of axons have a clear directional orientation [1–3]. In axons, the myelin, the microtubules and the neurofilaments are all structures that have the same directionality. Therefore, diffusion within axonal bundles is highly anisotropic [1–3] both on the macroscopic and microscopic levels.

First DWI was shown to be a very sensitive marker for cerebral ischemia [4,5] and then it was shown by Moseley et al., that water diffusion in WM is anisotropic [6]. Subsequently DTI was introduced [7] and shown to be extremely useful for studying white matter associated brain diseases [1–3,8]. DTI has also been applied to evaluate both normal and abnormal neuronal maturation in different species and in human subjects [9–19]. In the rat, for example, it is known that myelination starts after day 10 and peaks at about day 20 and decreases to some extent until day 45. After this stage myelination continues but at a low constant rate. Myelination leads to tissue compartmentalization, which may restrict the mobility of water molecules, therefore, should increase the FA value, measured by DTI [16]. The association between myelination and increase in FA in humans and in different animal models was reported in the literature [11,14,16,19,20]. However, other studies showed that this is not always the case as large FAs were observed in non myelinated nerves and in newborns before myelination occurs [21,22].

Despite the tremendous importance of DTI [1–3] it does suffer from some inherent limitations as it assumes that water diffusion in neuronal tissues is Gaussian. However it is well known that at high diffusion weighting and sufficient long diffusion times, the water signal decay does not obey the Stejskal Tanner equation [23,24]. For such high b-value diffusion data we suggested to use the q-space approach [25,26] to image diffusion in neuronal tissues [27–30]. This technique which does not assume any model of diffusion and is generally acquired with high diffusion weighting is more sensitive to slower diffusing water molecules and should, in principle, be more suitable for detecting restricted diffusion. Therefore q-space diffusion MR imaging (QSI) may be more suitable for detecting white matter associated disorders and for providing microstructural information on axonal architecture [28,31,32].

Indeed, in recent years we and others have used QSI to study different white matter associated disorders in both animals and human subjects [19,28–30,33–36]. For example, Farrell et al. used QSI to study spinal cords of MS patients [33,34] and we used QSI to study the brains of MS patients [28,29], the spinal cord of EAE swine [35] as well as rat spinal cord following trauma [36]. Recently, Biton et al. have demonstrated that QSI can distinguish between the spinal cords of myelin deficient (*md*) rat and their controls, in vitro [37,38]. Despite the widespread use of DTI and the increase use of QSI very few studies

have compared the methods in the same experimental model. Indeed, DTI was used to study different models of dysmyelination and demyelination [19,37–43]. Recently, Bar-Shir et al. used QSI and DTI to study the brains of the *md* rat [44], a model of dysmyelination, and Wu et al. very recently used the shaking canine (*sh*) pup, a large animal myelin mutant, to compare the sensitivity of high b-value q-space diffusion imaging and DTI in this experimental model of dysmyelination [19]. In the present study, we have used QSI and DTI to study in vitro the maturation in Long Evans shaker (*les*) rat brains and their age-matched controls at different stages of maturation. The *les* rat is a long-lived (up to 9 months old) autosomal recessive dysmyelinating mutant [45] characterized by a profound oligodendrocyte dysfunction as a result of a mutation in the myelin basic protein (MBP) gene [46] which results in rats having practically no myelin at old age [45,46].

2. Materials and methods

2.1. Sample preparation

This study was approved by the Animal Care Committee of the School of Veterinary Medicine of the University of Wisconsin-Madison. A total of 22 *les* and controls rats at the age of 20, 33 and 180 days were used in this study. The 20 and 180 day groups consisted each of three controls and *les* brains while the 33 day group consisted of five *les* and five control brains. Control and *les* rats were perfused with 0.1 mM PBS followed by paraformaldehyde (PFA) buffered in 0.1 mM PB (4% PFA). After perfusion, brains were excised and stored in 4% PFA. Twenty-four hours before the MR experiments, the excised brains were immersed in PBS solution in order to remove the paraformaldehyde. The brains were then placed in NMR tubes containing Fluorinert solutions (Sigma Chemical Co., St. Louis, MO, USA).

2.2. Diffusion MRI experiments

MRI experiments were performed using a 7 T/30 cm BioSpec System (Bruker, Germany) equipped with a BGU20 gradient system capable of producing x, y and z pulse gradients of 40 G cm^{-1}. Ten coronal continuous 1 mm slices were acquired with a protocol that included the acquisition of T2 weighted MR images (TR/TE = 3000/80 ms) and high b-value q-space diffusion MRI (QSI) data using a diffusion stimulated echo sequence. The following parameters were used when acquiring the QSI: TR/TE = 2500/20 ms, Δ = 100 ms, Δ = 4 ms, an FOV of 1.92 × 1.92 cm, a matrix of 128 × 64 (zero filled to 128 × 128) and 4 averages. The diffusion gradients were incremented from 0 to 36 G/cm in 16 equal steps for all 6 directions, resulting in maximal b- and q- values of 14,924 s/mm^2 and 613 cm^{-1}, respectively.

2.3. Image processing

After the MRI protocol was completed the raw data were analyzed using an in-house Matlab® program tool.

2.4. QSI image analysis

The QSI raw data were analyzed using the QSI methodology described in Ref. [27]. After Fourier transformation of the signal decay with respect to *q*, three different QSI indices were

extracted for each voxel, resulting in three QSI maps: the mean displacement map (in microns), the probability for zero displacement map (in arbitrary units (a.u.)), and the kurtosis map (a.u. in percent). The displacement values reported here are 0.425 times the FWHM of the displacement distribution profile [26]. For the displacement maps, the smallest mean displacement value out of the six diffusion directions was selected for each voxel in the map. For the probability maps, the highest probability for the zero displacement value out of the six diffusion directions was selected for each voxel in the map. The kurtosis maps were calculated according to [47]. For the kurtosis maps, the highest kurtosis value, which characterizes the deviation from Gaussian diffusion, i.e., maximum restriction, out of the six diffusion directions, was selected for each voxel in the map.

2.5. DTI image analysis

DTI indices, i.e., FA, λ_1, λ_2 and λ_3 were calculated according to Ref. [48] from the QSI data by analyzing the signal decay for b values of about 1000 s/mm^2. To make sure that QSI and DTI experimental parameters, besides the diffusion weighting, are *exactly* the same (TR,TE,Δ,δ, pulse sequence, crusher, RF pulses, acquisition time etc.,) the DTI indices were computed from the first points in each directions of the QSI data set. It should be noted, however, that the cost of such an experimental design is that the SNR of the DTI data set is smaller than that of the QSI data set.

2.6. ROI analysis

Three WM ROIs from three regions of the rat brain were selected in order to quantify the differences between the control and *les* groups. These ROIs represent the external capsule (*ec*), the corpus callosum (*cc*) and the internal capsule (*ic*). The examined ROIs were determined on the corresponding FA map of each brain and were then copied to the other diffusion maps. This procedure was performed on each examined sample and the average value of the examined index was extracted for each ROI.

27.7. Voxel-based analysis (VBA)

The Statistical Parametric Mapping (SPM2) program was also used to compare the *les* and the control groups for both the QSI and DTI results. First, a co-registration procedure with a displacement map of one representative control brain as template was applied for each diffusion (QSI or DTI) data set, i.e., displacement, probability, kurtosis, FA, λ_1, λ_2, and λ_3 maps. After the co-registration procedure was completed, we used the voxel base analysis (VBA) procedure to compare the *les* and control groups. Regions that expressed a statistical difference ($P < 0.005$) after a one-way-ANOVA test between the groups were highlighted on the displacement map template.

2.8. Statistical analysis

Statistical analysis was performed using the Student's t-test and $p \leq 0.05$ was taken as statistically significant changes.

2.9. Immunohistochemistry

Following perfusion, brains were dissected and fixed overnight in 4% PFA followed by cryoprotection in sucrose. The brain tissue was cut into 20 μm free-floating, transverse sections and incubated overnight with a rabbit anti MBP antibody (1:1000, Millipore) or a rabbit anti proteolipid protein (PLP) antibody (1:30,000, generous gift from Dr. Ian Griffiths). Immunohistochemistry was performed according to a standard colorimetric protocol using diaminobenzidine (DAB) to visualize labeling. Whole brain images were taken using a Nikon digital camera (N150) mounted on a Veblon tripod (VGB-37) above a standard light box.

3. Results

Fig. 1 (A, B and C) shows three slices of displacement, probability and kurtosis maps of a representative control brain in the three age groups obtained from QSI. This figure clearly shows that white matter (WM) areas show lower values of displacement and higher values of probability and kurtosis, in comparison with gray matter (GM) areas, as expected, implying that water diffusion is more restricted in WM areas than in GM areas. In addition, we observed that WM areas which are characterized by lower displacements and higher probability and kurtosis become larger and more emphasized as the brain matures. Fig. 2 shows the same data but for representative *les* brains. Here, WM areas also show lower displacement values and higher probability and kurtosis values as compared to GM areas, as seen in the control brains (Fig. 1). In terms of the progression with age, contrary to what was observed for the control brains, in the *les* brains WM areas, characterized by low mean displacement, high probability and high kurtosis, seem very similar in all age groups and do not show the same increase in areas as in the control brains. This finding implies that water diffusion is not very different in the WM areas of the *les* brains in all age groups. To better demonstrate the differences in the diffusion characteristics of the two groups we performed a detailed analysis in three different WM regions of interest (ROIs, see Fig. 1D for the definition of the ROIs used in quantitative analysis). The results of these analyses of the QSI and DTI data are summarized graphically in Figs. 3 and 4, respectively, for the internal capsule (*ic*) while the numerical values extracted for all three ROIs analyzed are presented in Tables 1 and 2.

Fig. 3 shows that all QSI indices in the internal capsule ROI are significantly different for the *les* group compare to their age-matched controls. This is even true for the immature 20 day old groups. We found that the mean displacements in the internal capsules are higher for the *les* groups as compared to their age-matched controls (Fig. 3A) while the probability for zero displacement and the kurtosis are smaller in the *les* group (Fig. 3B and C) at all age groups. In addition, the different QSI indices are similar for the 20 and 33 day old control brains. However, a significant change is observed in all three indices for the 180 day old control brains. In the *les* group we found nearly no change in the three QSI indices in the internal capsule with aging from day 20 to day 33 as in the control groups. However we found a statistically significant difference between day 33 and day 180 *les* groups but only in the mean displacement. All these observations imply that the water diffusion in the internal capsule in the control brains is more restricted than that of the *les* group, suggesting that the

myelin content in the internal capsules of the control brains is larger than that of the *les* group. These results also imply that water diffusion is more restricted in the older brains, in both control and *les* groups.

Fig. 4A shows the average FA, extracted from DTI originating from the exact same acquisitions, of the controls and *les* brains in the internal capsule and in three age groups. It was found that the controls have larger FA values than the *les*, in all age groups. However the difference between the control and *les* groups was found to be statistically significant only for the 33 day group and even there the statistical significance was found to be relatively low. We also analyzed the eigenvalues, extracted from the DTI, and found that indeed all eigenvalues are higher in the *les* brains as compared to their age matched controls, but the differences were of no or low statistical significance.

We also analyzed ROIs in the corpus callosum (*cc*) and the external capsule (*ec*). Tables 1 and 2 summarize the QSI and DTI indices, for the control and *les* brains in the three age groups for the three WM ROIs. The comparisons of the numerical values presented in Tables 1 and 2 show that, under the experimental design of the present study, the differences in the QSI indices between the control and *les* brains are generally larger than those of the DTI indices. The differences of all QSI indices between *les* and controls are highly significant while the differences in the DTI indices are generally relatively small with low statistical significance. We found statistically significant differences in the QSI indices of the *les* and control brains even for the 20 day age groups. For the DTI analysis, it is clear that the FA is the less effective index while λ_3 is the best index to detect the *les* pathology.

Fig. 5 shows a statistical comparison of the control and *les* groups using the SPM2 program for the 33 day old groups. Here, a one-way ANOVA test is performed on the two co-registered groups (control and *les*) and the statistically different voxels are highlighted. The analysis was done on all data sets extracted from either the QSI or DTI, i.e., displacement, probability, kurtosis, FA, λ_1, λ_2, and λ_3 maps. Fig. 5 shows representative group analysis performed on the probability, FA and λ_3 maps for the 33 day old groups only since we were not able to obtain more than 3 *les* brains of 180 day old rats due to extreme difficulties in keeping them alive up to this age. A group of 3 subjects is too small a group to allow one to perform such an SPM analysis reliably. The highlighted regions represent the ROIs which are significantly different between the two groups with $p < 0.005$. Significant differences were found in the probability maps and to some extent in λ_3 maps. Surprisingly, no significant differences were found for FA values. This implies that the FA index could not distinguish between control and *les* brains with high significance.

Fig. 6 shows myelin basic protein (MBP) and proteolipid protein (PLP) immunostained brain slices of 180 day old control and *les* rats. Both MBP and PLP are structural proteins in the myelin sheath that can be used to illustrate the myelin content of tissue. The MBP stained *les* brain shows no staining in comparison to its control, as *les* rats lack the MBP gene. However, PLP is still expressed within the cytoplasm of *les* oligodendrocytes. Therefore, although the *les* brain lacks myelin, PLP immunolabeling appears similar between the control and *les* brains.

4. Discussion

In the present study QSI and DTI were used, for the first time, to study in vitro the *les* rat brains, and their age-matched controls in different stages of maturation. To be able to compare the sensitivity of QSI and DTI indices for this pathology of dysmyelination and at different stages of maturation the same acquisition was used to compute the QSI and DTI indices implying also that the SNR of the DTI is somewhat smaller than that of the QSI. Quantitative analysis of the QSI and DTI indices is reported in three ROIs (i.e., the corpus callosum (*cc*), internal capsule (*ic*), external capsule (*ec*)). In addition, SPM2 was used for voxel based analysis of the difference of both groups but only for the 33 day old group where the size of the group permitted such analysis to be performed. This enabled us to evaluate the ability of the QSI and DTI indices to detect the *les* pathology on the one hand, and to evaluate the ability of each methodology to follow both normal and abnormal maturation on the other hand.

The QSI indices were capable of significantly distinguishing between the *les* and control groups, in all age groups and in all of the ROIs examined. Only in the cc ROI at the 20 day old age group were the differences between the QSI indices of the *les* and controls not statistically significant. The QSI displacement values were found to be lower while the probability for zero displacement and kurtosis values were found to be higher in the WM ROIs of the control brains in comparison with the *les* brains. These results are in line with previous QSI studies of dysmyelination and demyelination [19,33–35,37,38] and indicate a higher level of restricted diffusion in the WM of the control brains compared with the *les* brains. The QSI indices showed significant differences between the 33 and 180 age groups in the control brains. There a significant decrease was found in the displacement values and a significant increase was found in both the probability for zero displacement and kurtosis values. However in the control group the differences between the QSI indices of the 20 and 33 day groups were not statistically significant. This implies that a higher level of restricted diffusion is present in the older control brains, compared to the young aged ones — a manifestation of normal maturation. In the *les* brains, the differences were largely insignificant. Only in the internal capsules was the decrease in the displacement between the 33 and 180 age groups found to be statistically significant. This indicates a lower degree but still significant restricted diffusion in the older *les* brains. This demonstrates that some degree of restriction is still observable in the 180 *les* brains where histology shows very little myelin as depicted in Fig. 6. These results are in line with previous studies that demonstrated that myelin does affect water restriction and hence diffusion anisotropy but it is not a prerequisite for the observation of such diffusion restriction and anisotropy [37,41,44].

In the present study, the DTI indices could not distinguish between the control and *les* groups in most of the examined cases. FA values extracted from DTI were found to be smaller in the *les* group as compared to controls while the eigenvalues were, in general, higher in the *les* groups. However, none of the DTI indices could detect the *les* pathology at the 20 day old group and only for the 33 day groups, where the group size was larger, were the differences in the FA values statistically significant. Even there the statistical significance was relatively low. The eigenvalues were generally higher in the *les* groups as

compared to their age-matched controls and there the statistical significance was somewhat higher for λ_2, and λ_3 as compared to the FA. We observed that λ_3, which was found to be the most efficient DTI index for detecting the *les* pathology, was able to detect this pathology also in the 180 day groups. The differences between the groups are expected to be more accentuated with age, as the normal brains become more myelinated and mature. Indeed in line with this expectation, the FA values were larger in the controls of all age groups although a statistically significant difference was found only in the internal capsule and only for the 33 day age group. These results imply that under our experimental conditions FA values cannot distinguish between the groups even in the brains of the 180 day old rats. The FA values average the changes of the three eigenvalues λ_1 ($\lambda_{\|}$), λ_2, and λ_3 ($\lambda_{\perp}$). As all three eigenvalues are larger in the *les* brains compared to the control brains, the changes in FA values are suppressed. In the cases where all eigenvalues change in the same direction one should expect the FA values to have a lower prognostic power as found in the present study. The VBA maps calculated with SPM support the ROIs based results. Fig. 5 shows no significant differences between the groups when FA maps with a threshold of $p < 0.005$ were used. The DTI λ_3 map, however, shows small areas with significant differences and the QSI based map (i.e. probability) shows the biggest area of significant differences and seems to be the best measure for distinguishing between the *les* and control brains. These results seem to suggest that QSI indices are more sensitive to this WM pathology than DTI indices in line with the results of recent studies which compared QSI and DTI in other WM mutants [19,38]. It should be noted that our experimental design implies that the SNR of the DTI data is lower than in the QSI data, however it seems to us that the higher efficiency to the QSI indices, found in the present study, originates primarily from the higher diffusion weighting of the QSI data which makes it more sensitive the restricted diffusion.

It has been suggested that a decrease in axial diffusivity ($\lambda_{\|}$) of the diffusion tensor reflects axonal degeneration while an increase in the radial diffusivity ($\lambda_{\perp}$) is more associated to demyelination [19,39,43]. Here, in line with histology that shows massive dysmyelination with relatively little effect on axonal membrane, we found an increase in both the radial and axial diffusivity in line with other recent studies [19,38].

In the present study a relatively long diffusion time of 100 ms was used to allow the water molecules to explore larger distances and to enhance the effect of restricting barriers on the signal attenuation. Although QSI clearly demonstrated that a diffusion time of about 6–7 ms is sufficient to observe significant restriction in optic nerve for example [49], we and others have recently shown that longer diffusion times result in higher apparent anisotropy [38] and provide better means to distinguish abnormal WM from normal WM [38,43,44].

In conclusion, we showed that all QSI indices are very efficient in detecting the *les* pathology of dysmyelination and at all age groups. We found that the FA, extracted from DTI, is less efficient than the eigenvalues in detecting the *les* pathology. Since the DTI and QSI indices were collected from the same acquisition with exactly the same experimental conditions one can argue that it is probably the diffusion weighting in addition to the somewhat higher SNR which is responsible for the higher diagnostic power of the QSI indices. Indeed, QSI based indices obtained at high b or q-values have high diagnostic power in this model of dysmyelination.

Acknowledgments

The animal MRI scanner used in the present study was purchased with aid of the ISF (Israel Science Foundation, Jerusalem) and the Raymond and Beverly Sackler Center of Biophysics of Tel Aviv University and is operated under the Federico Strauss Center for Computational NeuroImaging of Tel Aviv University.

References

[1]. Van Zijl PCM, Le Bihan D. Diffusion tensor imaging and axonal mapping. NMR Biomed. 2002; 15:431–593. [PubMed: 12489093]

[2]. Johansen-Berg, H.; Behrens, TEJ., editors. Diffusion MRI: from quantitative measurement to in vivo neuroanatomy. Academic Press; London, UK: 2009.

[3]. Jones, DK., editor. Diffusion MRI: theory, methods and applications. Oxford University Press; New York: 2011.

[4]. Moseley ME, Cohen Y, Mintorovitch J, Chileuitt L, Shimizu H, Kucharczyk J, et al. Early detection of regional cerebral-ischemia in cats — comparison of diffusion-weighted and T2-weighted MRI and spectroscopy. Magn Reson Med. 1990; 14:330–46. [PubMed: 2345513]

[5]. Lansberg MG, Norbash AM, Marks MP, Tong DC, Moseley ME, Albers GW. Advantages of adding diffusion-weighted magnetic resonance imaging to conventional magnetic resonance imaging for evaluating acute stroke. Arch Neurol. 2000; 57:1311–6. [PubMed: 10987898]

[6]. Moseley ME, Cohen Y, Kucharczyk J, Mintorovich J, Asgari HS, Wedland MF, et al. Diffusion weighted MR imaging of anisotropic water diffusion in cat central nervous system. Radiology. 1990; 176:439–45. [PubMed: 2367658]

[7]. Basser PJ, Mattiello J, Le Bihan D. MR diffusion tensor spectroscopy and imaging. Biophys J. 1994; 66:259–67. [PubMed: 8130344]

[8]. Nakahara M, Ericson K, Bellander BM. Diffusion-weighted MR and apparent diffusion coefficient in the evaluation of severe brain injury. Acta Radiol. 2001; 42:365–9. [PubMed: 11442459]

[9]. Huppi PS, Maier SE, Peled S, Zientara GP, Barnes PD, Jolesz FA, et al. Microstructural development of human newborn cerebral white matter assessed in vivo by diffusion tensor magnetic resonance imaging. Pediatr Res. 1998; 44:584–90. [PubMed: 9773850]

[10]. Prayer D, Prayer L. Diffusion-weighted magnetic resonance imaging of cerebral white matter development. Eur J Radiol. 2003; 45:235–43. [PubMed: 12595108]

[11]. Partridge SC, Mukherjee P, Henry RG, Miller SP, Berman JI, Jin H, et al. Diffusion tensor imaging: serial quantitation of white matter tract maturity in premature newborns. Neuroimage. 2004; 22:1302–14. [PubMed: 15219602]

[12]. Ben Bashat D, Ben Sira L, Graif M, Pianka P, Hendler T, Cohen Y, et al. Normal white matter development from infancy to adulthood: comparing diffusion tensor and high b-value diffusion weighted MR images. J Magn Reson Imaging. 2005; 21:503–11. [PubMed: 15834918]

[13]. Huang H, Zhang J, Wakana S, Zhang W, Ren T, Richards LJ, et al. White and gray matter development in human fetal, newborn and pediatric brains. Neuroimage. 2006; 33:27–38. [PubMed: 16905335]

[14]. Bockhorst KH, Narayana PA, Liu R, Ahobila-Vijjula P, Ramu J, Kamel M, et al. Early postnatal development of rat brain: in vivo diffusion tensor imaging. J Neurosci Res. 2008; 86:1520–8. [PubMed: 18189320]

[15]. Mori S, Itoh R, Zhang JY, Kaufmann WE, Van Zijl PCM, Solaiyappan M, et al. Diffusion tensor imaging of the developing mouse brain. Magn Reson Med. 2001; 46:18–23. [PubMed: 11443706]

[16]. Verma R, Mori S, Shen D, Yarowsky P, Zhang J, Davatzikos C. Spatiotemporal maturation patterns of murine brain quantified by diffusion tensor MRI and deformation-based morphometry. Proc Natl Acad Sci. 2005; 102:6978–83. [PubMed: 15860588]

[17]. Baratti C, Barnett AS, Pierpaoli C. Comparative MR imaging study of brain maturation in kittens with T1, T2, and the trace of the diffusion tensor. Radiology. 1999; 210:133–42. [PubMed: 9885598]

[18]. D'Arceuil H, Liu C, Levitt P, Thompson B, Kosofsky B, de Crespigny A. Three dimensional high-resolution diffusion tensor imaging and tractography of the developing rabbit brain. Dev Neurosci. 2008; 30:262–75. [PubMed: 17962716]

[19]. Wu Y, Field AS, Duncan I, Samsonov AA, Kondo Y, Tudorascu D, et al. High b-value and diffusion tensor imaging in a canine model of dysmyelination and brain maturation. Neuroimage. 2011; 58:829–37. [PubMed: 21777681]

[20]. Cheung MM, Hui ES, Chan KC, Helpern JA, Qi L, Wu EX. Does diffusion kurtosis imaging lead to better neural tissue characterization? A rodent brain maturation study. Neuroimage. 2009; 45:386–92. [PubMed: 19150655]

[21]. Beaulieu C, Allen PS. Determinant of anisotropic water diffusion in the nerves. Magn Reson Med. 1994; 31:394–400. [PubMed: 8208115]

[22]. Beaulieu C. The basis of anisotropic water diffusion in the nervous system—a technical review. NMR Biomed. 2002; 15:435–55. [PubMed: 12489094]

[23]. Niendorf T, Dikhuizen RM, Norris DG, van Lookeren Campagne M, Nicolay K. Biexponential diffusion attenuation in various states of brain tissue: implications to diffusion-weighted imaging. Magn Reson Med. 1996; 36:847–57. [PubMed: 8946350]

[24]. Assaf Y, Cohen Y. Non mono-exponential attenuation of the water and N-acetylaspartate signals due to diffusion in brain tissue. J Magn Reson. 1998; 131:69–85. [PubMed: 9533908]

[25]. Callaghan PT, Macgowan D, Packer KJ, Zelaya FO. High resolution q-space imaging in porous structures. J Magn Reson. 1990; 90:177–82.

[26]. Cory DG, Garroway AN. Measurement of translational displacement probabilities by NMR — an indicator of compartmentation. Magn Reson Med. 1990; 14:435–44. [PubMed: 2355827]

[27]. Assaf Y, Mayk A, Cohen Y. Displacement imaging of spinal cord using q-space diffusion weighted MRI. Magn Reson Med. 2000; 44:713–22. [PubMed: 11064406]

[28]. Cohen Y, Assaf Y. High b-value q-space analyzed diffusion-weighted MRS and MRI in neuronal tissues — a technical review. NMR Biomed. 2002; 15:516–42. [PubMed: 12489099]

[29]. Assaf Y, Ben-Bashat D, Chapman J, Peled S, Biton IE, Kafri M, et al. High b-value q-space analyzed diffusion weighted MRI: application to multiple sclerosis. Magn Reson Med. 2002; 47:115–26. [PubMed: 11754450]

[30]. Assaf Y, Mayzel-Oreg O, Gigi A, Ben-Bashat D, Mordohovitch M, Verchovsky R, et al. High b-value q-space analyzed diffusion MRI in vascular dementia: a preliminary study. J Neurol Sci. 2002; 203:235–9. [PubMed: 12417390]

[31]. Ong HH, Wright AC, Wherli SL, Souza A, Schwartz ED, Hwang SN, et al. Indirect measurement of regional axon diameter in excised mouse spinal cord with q-space imaging: simulation and experimental studies. Neuroimage. 2008; 40:1619–32. [PubMed: 18342541]

[32]. Ong HH, Wehrli FW. Quantifying axon diameter and intra-cellular volume fraction in excised mous spinal cord with q-space imaging. Neuroimage. 2010; 51:1360–6. [PubMed: 20350604]

[33]. Farrell JAD, Smith SA, Gordon-Lipkin EM, Reich DS, Calabresi PA, van Zijl PCM. High b-value q-Space diffusion-weighted MRI of the human cervical spinal cord in vivo: feasibility and application to multiple sclerosis. Magn Reson Med. 2008; 59:1079–89. [PubMed: 18429023]

[34]. Farrell JAD, Zhang J, Jones MV, DeBoy CA, Hoffman PN, Landman BA, et al. q-Space and conventional diffusion imaging of axon and myelin damage in the rat spinal cord after axotomy. Magn Reson Med. 2008; 59:1079–89. [PubMed: 18429023]

[35]. Biton IE, Mayk A, Kidron D, Assaf Y, Cohen Y. Improved detectability of experimental allergic encephalomyelitis in excised swine spinal cords by high b-value q-space DWI. Exp Neurol. 2005; 195:437–46. [PubMed: 16098966]

[36]. Nossin-Manor R, Duvdevani R, Cohen Y. q-Space high b-value diffusion MRI of hemi-crush in rat spinal cord: evidence for spontaneous regeneration. Magn Reson Imaging. 2002; 20:231–41. [PubMed: 12117605]

[37]. Biton IE, Duncan ID, Cohen Y. High b-value q-space diffusion MRI in myelin deficient rat spinal cords. Magn Reson Imaging. 2006; 24:161–6. [PubMed: 16455404]

[38]. Biton IE, Duncan ID, Cohen Y. q-Space diffusion of myelin-deficient spinal cords. Magn Reson Med. 2007; 58:993–1000. [PubMed: 17969109]

[39]. Song SK, Sun S, Ramsbottom MJ, Chang C, Russell J, Cross AH. Dysmyelination revealed through MRI as increased radial (but unchanged axial) diffusion of water. Neuroimage. 2002; 17:1429–36. [PubMed: 12414282]

[40]. Ono J, Harada K, Takahashi M, Maeda M, Ikenaka K, Sakurai K, et al. Differentiation between dysmyelination and demyelination using magnetic resonance diffusional anisotropy. Brain Res. 1995; 671:141–8. [PubMed: 7728526]

[41]. Gulani V, Webb AG, Duncan ID, Lauterbur PC. Apparent diffusion tensor measurements in myelin-deficient rat spinal cords. Magn Reson Med. 2001; 45:191–5. [PubMed: 11180424]

[42]. Tyszka JM, Readhead C, Bearer EL, Paulter RG, Jacobs RE. Statistical diffusion tensor histology reveals regional dysmyelination effects in the shiverer mouse mutant. Neuroimage. 2006; 21:1058–65. [PubMed: 16213163]

[43]. Nair G, Tanahashi Y, Low HP, Bilings-Gagliardi S, Schwartz WJ, Dong TQ. Myelination and long diffusion time alter diffusion-tensor imaging contrast in myelin deficient shiverer mice. Neuroimage. 2005; 28:1650174.

[44]. Bar-Shir A, Duncan ID, Cohen Y. QSI and DTI of excised brains of the myelindeficient rat. Neuroimage. 2009; 48:109–16. [PubMed: 19539038]

[45]. Kwiecien JM, O'Connor LT, Goetz BD, Delaney KH, Fletch AL, Duncan ID. Morphological and morphometric studies of the dysmyelinating mutant, the Long Evans shaker rat. J Neurocytol. 1998; 27:581–91. [PubMed: 10405025]

[46]. O'Connor LT, Goetz BD, Kwiecien JM, Delaney KH, Fletch AL, Duncan ID. Insertion of retrotransposon in Mbp disrupts mRNA spicing in a new rat mutant. J Neurosci. 1999; 19:3404–13. [PubMed: 10212300]

[47]. Jensen JH, Helpern JA, Ramani A, Lu HZ, Kaczynski K. Diffusional kurtosis imaging: the quantification of non-Gaussian water diffusion by means of magnetic resonance imaging. Magn Reson Med. 2005; 53:1432–40. [PubMed: 15906300]

[48]. Basser PJ, Pierpaoli C. Microstructural and physiological features of tissues elucidated by quantitative diffusion tensor MRI. J Magn Reson B. 1996; 111:209–19. [PubMed: 8661285]

[49]. Bar-Shir A, Cohen Y. High b-value q-space diffusion MRS of nerve: structural information and comparison with histological evidence. NMR Biomed. 2008; 21:165–74. [PubMed: 17492659]

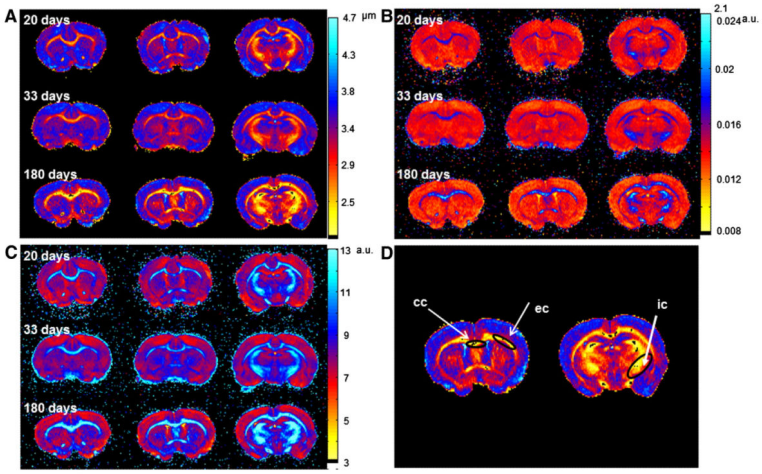

Fig. 1.

Three slices of displacement (A), probability (B) and kurtosis (C) maps of a representative control brain, obtained from the QSI experiments. Panel (D) shows the ROIs used for the quantitative analysis presented in Figs. 3 and 4 and in Tables 1 and 2.

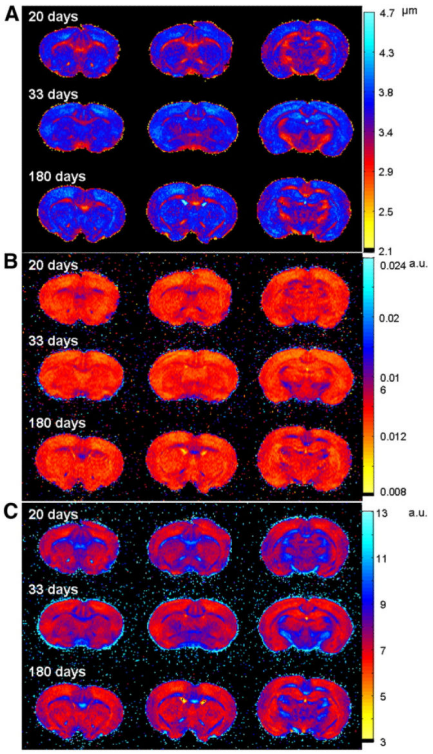

Fig. 2.

Three slices of displacement (A), probability (B) and kurtosis (C) maps of a representative *les* brain, obtained from the QSI experiments.

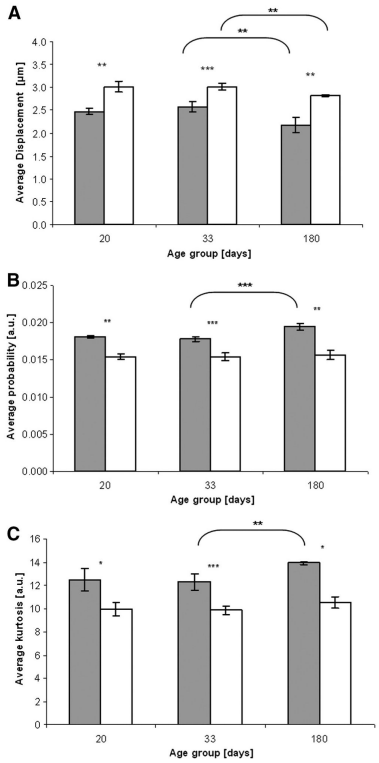

Fig. 3.

Average minimal displacement (A), maximal probability (B) or maximal kurtosis (C) values of control (black columns) and *les* (white columns) in the internal capsule (ic) and in the three examined age groups. n = 3 in the 20 and 180 day old groups, n = 5 in the 33 day old group, *p < 0.05, **p < 0.005, ***p < 0.0005.

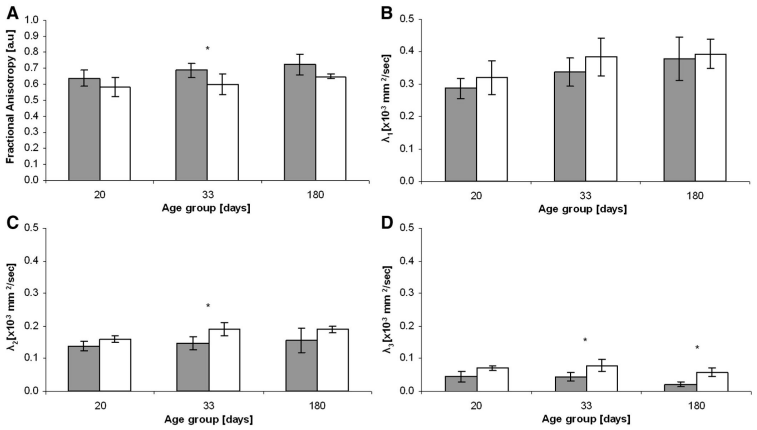

Fig. 4.

Average fractional anisotropy (A), λ_1 (B), λ_2 (C) and λ_3 (D) values of control (black columns) and *les* (white columns) in the internal capsule (ic) in the three examined age groups. n = 3 in the 20 and 180 day old groups, n = 5 in the 33 day old group, *p < 0.05.

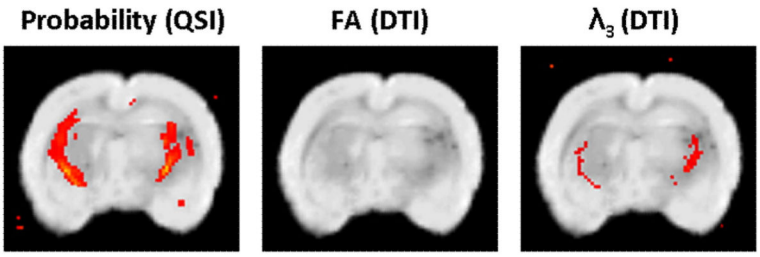

Fig. 5.

Results from the VBA procedure performed by the SPM2 on the *les* and control brains of the 33 day old group for three indices: probability values extracted from QSI measurements, FA and λ_3, all extracted from DTI data. Highlighted regions represent regions with a significant difference ($p < 0.005$) between the control and *les* groups.

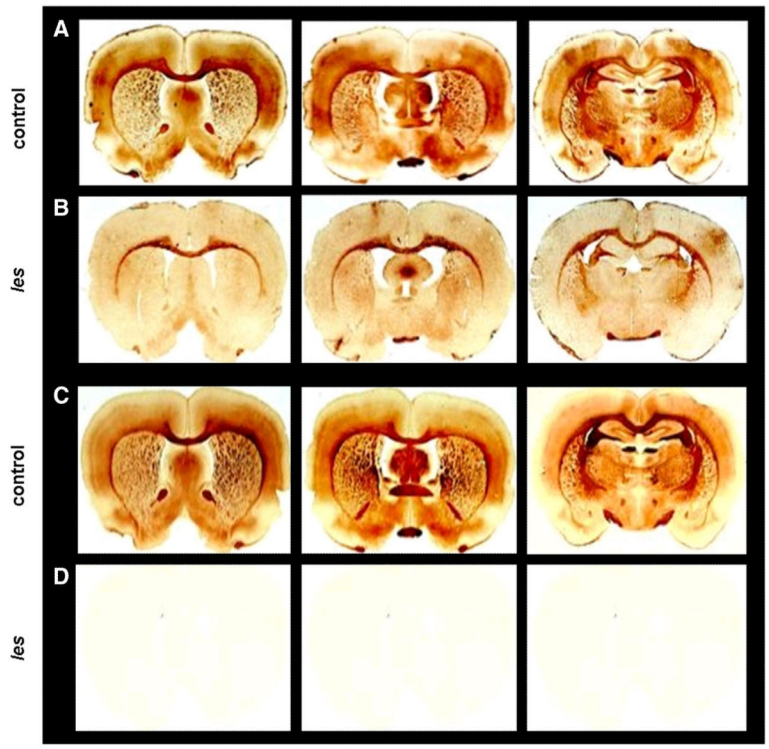

Fig. 6.

Histological slices from a 180 day old control brain immunostained with PLP (A) or MBP (C) and a 180 day old *les* brain immunostained with PLP (B) or MBP (D).

Table 1

Average values of QSI indices, minimal displacement, maximal probability, maximal kurtosis in the corpus callosum (cc), external capsule (ec) and internal capsule (ic) of controls and *les* brains of the three age groups and the extracted p-values.

Rat age [days]	ROI	Minimum displacement [μm]			Maximal probability [a.u.]			Maximal kurtosis [a.u.]		
		Control	*les*	P-values	Control	*les*	P-values	Control	*les*	P-values
20	cc	2.7 ± 0.1	2.8 ± 0.1	0.620	0.018 ± 0.0006	0.016 ± 0.0110	0.095	12.1 ± 1.0	11.2 ± 0.8	0.301
	ec	2.8 ± 0.1	3.3 ± 0.1	0.010	0.016 ± 0.0010	0.010 ± 0.0003	0.070	11.2 ± 0.8	8.7 ± 0.2	0.030
	ic	2.5 ± 0.1	3 ± 0.1	0.003	0.015 ± 0.0004	0.018 ± 0.0003	0.005	12.5 ± 1.0	10 ± 0.6	0.025
33	cc	2.7 ± 0.2	3.2 ± 0.1	0.002	0.017 ± 0.0010	0.015 ± 0.0005	0.008	11.2 ± 1.0	9.2 ± 0.3	0.007
	ec	2.9 ± 0.1	3.3 ± 0.2	0.005	0.020 ± 0.0010	0.010 ± 0.0010	0.017	10.7 ± 0.7	8.9 ± 0.7	0.004
	ic	2.6 ± 0.1	3 ± 0.1	0.0003	0.018 ± 0.0003	0.015 ± 0.0005	0.00004	12.3 ± 0.7	9.9 ± 0.4	0.0003
180	cc	2.3 ± 0.1	3.1 ± 0.2	0.009	0.020 ± 0.0007	0.015 ± 0.0013	0.024	13.5 ± 0.5	9.7 ± 1.1	0.017
	ec	2.6 ± 0.1	3.4 ± 0.3	0.019	0.020 ± 0.0004	0.014 ± 0.0009	0.011	12.2 ± 0.4	8.2 ± 1.0	0.010
	ic	2.2 ± 0.2	2.8 ± 0.1	0.0009	0.019 ± 0.0004	0.016 ± 0.0006	0.003	13.9 ± 0.1	10.5 ± 0.5	0.006

Table 2

Average values of DTI indices, i.e. FA and $\lambda 1$, $\lambda 2$ and $\lambda 3$ extracted for the internal capsule (ic), external capsule (ec) and corpus callosum (cc) of controls and *les* brains in the three age groups.

Rat age [days]	ROI	FA			$\lambda 1$ [$\times 10^3$ mm^2/s]			$\lambda 2$ [$\times 10^3$ mm^2/s]			$\lambda 3$ [$\times 10^3$ mm^2/s]		
		Control	*les*	P-values	Control	*les*	P-values	Control	*les*	P-values	Control	*les*	P-values
20	cc	0.67 ± 0.11	0.57 ± 0.05	0.26	0.32 ± 0.04	0.28 ± 0.03	0.23	0.12 ± 0.02	0.16 ± 0.02	0.05	0.10 ± 0.07	0.07 ± 0.03	0.50
	ec	0.57 ± 0.05	0.51 ± 0.05	0.19	0.28 ± 0.03	0.33 ± 0.03	0.08	0.16 ± 0.02	0.18 ± 0.02	0.16	0.07 ± 0.03	0.10 ± 0.004	0.17
	ic	0.64 ± 0.05	0.58 ± 0.06	0.30	0.29 ± 0.03	0.32 ± 0.05	0.41	0.14 ± 0.01	0.16 ± 0.01	0.11	0.05 ± 0.02	0.07 ± 0.01	0.08
33	cc	0.65 ± 0.07	0.58 ± 0.07	0.18	0.32 ± 0.05	0.41 ± 0.06	0.04	0.16 ± 0.01	0.21 ± 0.04	0.06	0.05 ± 0.02	0.09 ± 0.01	0.003
	ec	0.56 ± 0.04	0.50 ± 0.08	0.17	0.30 ± 0.02	0.36 ± 0.04	0.02	0.17 ± 0.02	0.24 ± 0.03	0.005	0.08 ± 0.02	0.10 ± 0.04	0.19
	ic	0.69 ± 0.05	0.60 ± 0.06	0.04	0.34 ± 0.04	0.38 ± 0.06	0.20	0.15 ± 0.02	0.19 ± 0.02	0.01	0.04 ± 0.01	0.08 ± 0.02	0.012
180	cc	0.72 ± 0.004	0.68 ± 0.01	0.58	0.38 ± 0.07	0.39 ± 0.05	0.71	0.16 ± 0.04	0.19 ± 0.01	0.12	0.04 ± 0.02	0.07 ± 0.03	0.21
	ec	0.59 ± 0.05	0.54 ± 0.12	0.40	0.32 ± 0.05	0.46 ± 0.11	0.13	0.18 ± 0.04	0.25 ± 0.04	0.03	0.08 ± 0.03	0.09 ± 0.05	0.55
	ic	0.72 ± 0.06	0.65 ± 0.02	0.06	0.38 ± 0.07	0.39 ± 0.05	0.71	0.16 ± 0.04	0.19 ± 0.01	0.12	0.02 ± 0.01	0.06 ± 0.01	0.02